DISCRETE ELEMENT METHOD FOR THE FAILURE ANALYSIS OF STEEL PIPES CROSSING ACTIVE FAULTS

Radan IVANOV[1] and Shiro TAKADA[2]

[1] Student of JSCE, Ph.D., Visiting Researcher, Engineering Department, Kobe University
(1-1 Rokkodai, Nada-ku, Kobe, Hyogo 650-8501)

[2] Fellow of JSCE, Dr.Eng., Professor, Engineering Department, Kobe University
(1-1 Rokkodai, Nada-ku, Kobe, Hyogo 650-8501)

A specialised DEM method for the failure analysis of shell structures made of steel is presented. Hereby, a shell is represented by an equivalent lattice. The in-plane stiffness of shells is represented by a lattice of energy equivalent normal springs, and the bending stiffness of walls is represented by bending springs. The ability of the method to simulate highly non-linear situations is demonstrated by an analysis of a cylinder pinched perpendicularly to its axis by a force couple. A case study was carried out on a pipe in the Fengyuan region in Taiwan that sustained damage during the Chi-Chi Earthquake.

Key Words: *Discrete element method, Shell structures, Steel pipes, Failure analysis*

1. INTRODUCTION

In the past ten years the world was hit by a number of destructive earthquakes; a few to mention, the Hanshin Earthquake in Japan, the Northridge Earthquake in the USA and the Chi-Chi Earthquake in Taiwan. With the rapid growth of infrastructure as part of built environment in our modern world the damage to lifeline facilities became important and impossible to neglect. Steel pipelines also sustained damage[1)], sometimes rather severe. Considering the ability of the DEM to perform well in situations of high non-linearity, both geometrical and material, we propose a modelling technique for failure analysis pertaining to shell structures in general and steel pipes in particular.

2. METHOD OF ANALYSIS

A multi-purpose 3-D DEM software was developed[2)] that can carry-out various types of geometrically and materially non-linear failure analyses in real time, e.g. fracture and collapse of bulky RC structures, global buckling and elasto-plastic analysis of space trusses, global and local buckling of space frames, failure analysis of cables and cable nets etc. The method presented in this work is a part of the above mentioned study. It relies on substituting a shell by an assembly of springs connecting nodes in the central surface. In doing so, the mechanisms by which shells carry loads have to be preserved. The internal forces appearing in shells upon loading are normal forces in the surface of shells and bending moments/shear forces. The equivalent lattice of springs has to be so designed as to its behaviour to resemble as closely as possible the behaviour of the actual shell. The way this is done is explained bellow.

(1) Representation of Normal Stiffness

The normal stiffness of the shell has to be represented by the cumulative axial stiffness of the springs in the assembly. We choose to use a regular triangular arrangement of the springs for simplicity of derivation. As a criterion for defining the stiffness of the springs we impose equality of the strain energy accumulated in the shell on one hand, and in the assembly of springs representing the shell on the other. Since we have only one set of springs (axial) to define, and as due to the regularity of the assembly the properties of all individual springs is identical, it is sufficient to consider only one stress-strain state. The most convenient stress-strain state is the uniform biaxial stress condition. Consider a plane square continuos region LxL with thickness t loaded by uniform stress σ and the same region substituted by normal springs distributed in an equilateral triangle fashion. For plain stress conditions the strains in the two principle directions ε_x and ε_y are the same, and by integrating over the region $LxLxt$ we obtain the total strain energy in the region V,

$$V = \iint_{LxL} dV = t\frac{\sigma^2}{E}(1-\nu)L^2 \qquad (1)$$

Next we have to find the strain energy of the region as substituted by springs with length D. A count of the number of springs in the region yields $n = 2\sqrt{3}\,L^2/D^2$. The strain energy V_1 accumulated in a single spring of stiffness k_n undergoing extension Δ is,

$$V_1 = \frac{1}{2}\Delta^2 k_n = \frac{1}{2}k_n[\frac{\sigma}{E}(1-\nu)D]^2 \quad (2)$$

Finally, the equation from which we define the spring stiffness is the equality of the strain energy in the continuous region and the strain energy in the spring system,

$$nV_1 = V \quad (3)$$

which after some algebra yields the expression for the spring system we seek[2],

$$k_n = \frac{\sqrt{3}}{3}\frac{tE}{(1-\nu)} \quad (4)$$

Finally, we compute the area of the spring A corresponding to the derived stiffness and the spring length,

$$A = \frac{Dk_n}{E} \quad (5)$$

(2) Representation of Bending Stiffness

Bending stiffness is included by introducing shear and rotational springs so that shear force F_i^s, and bending moment M_i in addition to the already considered normal force F_i^n could be transferred between neighbouring bodies. The relation between these forces and corresponding displacements for the endpoints i and j of a 3-D beam in a certain plane with second moment of inertia I in this plane can be expressed as follows,

$$F_i^s = \frac{12EI}{l^3}(x_i^s - x_j^s) - \frac{6EI}{l^2}(\theta_i - \theta_j) \quad (6)$$

$$M_i = \frac{6EI}{l^2}(x_i^s - x_j^s) - \frac{4EI}{l}(\theta_i - \frac{\theta_j}{2}) \quad (7)$$

with symmetric relations for node j. We use constant I in any plane passing through the axis of the beam and neglect torsion. With the adopted modelling by triangular lattice of beams the stiffness in the surface plane is mostly due to the action of normal forces in the beams, so flexure will tend to occur out of the plane only. Therefore we can assume the beams to have a constant I in all directions, which also leads to simplification of the calculation procedure and consequent time savings. The second moment of area has to be computed so as to represent the out-of-plane bending stiffness of the wall. There will be small parasite moments developing in the plane of shell but they can be neglected. In this sense the assumption of a single constant second moment of area is thought to be reasonable. For computing the second moment of inertia participating in Eqs. (6) and (7) we use the area A given by Eq. (5). From it we compute equivalent breadth $b=A/t$, and $I = bt^3/12$.

(3) Constitutive Model and Failure Criteria

Choosing steel as target material, bilinear hysteretic model with strain hardening was adopted as constitutive model and ultimate strain imposed as failure criterion for the deformation of axial springs[3]. The behaviour of the bending springs in the current version is elastic. In the future development of the method plastic deformations in bending will be represented by plastic hinge formation and failure criterion imposed in terms of ultimate rotation capacity of the plastic hinges.

(4) Solution Procedure

A body with mass m and mass moment of inertia J are assigned to each node. Their values are computed from the volume of shell surrounding the node. J is computed about an axis laying in the plane through the node, tangent to the shell. The numerical solution is based on the integration of the Newton equations of motion for each body. The motion of a body is considered uncoupled from the motion of the rest of the bodies during a single time step, thus eliminating the need to assemble a stiffness matrix. Each body then moves due to the out-of-balance force appearing on summation of the forces in all springs originating from it. For the system to reach equilibrium two types of damping are applied. First, the relative motion between bodies is damped by a coefficient of damping calculated from the critical damping ratio of the material. This is termed local damping. In addition small amount of viscous damping works on the absolute velocities of the objects. This is referred to as global damping and represents the resistance of the medium in which the structure stands. The procedure is inherently dynamic, geometrically non-linear, and can accommodate easily arbitrary amounts of rigid body motion.

3. PERFORMANCE

In order to demonstrate the ability of the analysis procedure to handle very large geometrical nonlinearity, a short cylindrical segment with height H= 2m, diameter D=2m and wall thickness 0.02m was pinched at two opposite points as shown in Fig. 1. In the end of the analysis the two points actually come together. As can be seen the same figure the shape of the cylinder changes drastically and signs of local buckling can be seen on the top and bottom end of the cylinder. Even with such large deformations the analyses proceeded smoothly.

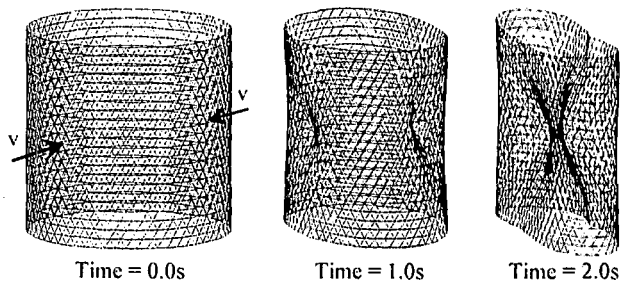

Fig. 1 Analysis of a pinched cylinder

4. CASE STUDY – FENGYUAN PIPE

(1) Features of the Model

The set-up for the analyses is shown in Fig. 2. A pipe segment 27m long with diameter D=2m and wall thickness t=0.019m, buried at depth 3.4m was analysed. The pipe was made of steel grade compatible with the Japanese STW 41[4], with yield point of 4.1×10^5 kN/m^2. Summary of all analyses is given in Table 1. Cases A1, A2 and A8 correspond to the actual pipe properties, and fault orientation. Apart from the original position of the pipe several analyses were performed on a fictitious new position at 90 degrees from the original one. Also, a smaller wall thickness of 0.015m corresponding to Japanese standards[4] for pipe diameter 2m was used in some of the analyses. The model was fixed at both ends and the fault motion simulated by applying a constant velocity at one of the pipe ends. The velocity is such that the total fault displacement occurs within 5s. The actual components of fault displacement at the site were used; NORTH=6.52m, WEST=2.75m and UP=3.01m. For three of the analyses pipe-soil interaction was considered by radial compression-only springs as shown in Fig. 3. The properties of the springs in the bottom part of the pipe were calculated following the guidelines of the Japanese manual for design of gas pipelines, where the stiffness per unit area is given by the formula[5],

$$k = \frac{1}{3} k_{30} \left(\frac{D}{17} \right)^{-3/4} \quad [\text{kgf/cm}^3] \qquad (8)$$

In the formula k_{30} is the stiffness produced by a standard test on soil specimen of diameter 30cm. The stiffness of the spring at the top part is assumed one third of the stiffness of the bottom springs[6]. The top spring were assumed to fail due to uplift at 10% strain. For analyses A7 and A8, k_{30}=3kgf/cm^3 corresponding to soil of medium to low stiffness, and for analysis A9 k_{30}=6kgf/cm^3 corresponding to medium to high stiffness were used.

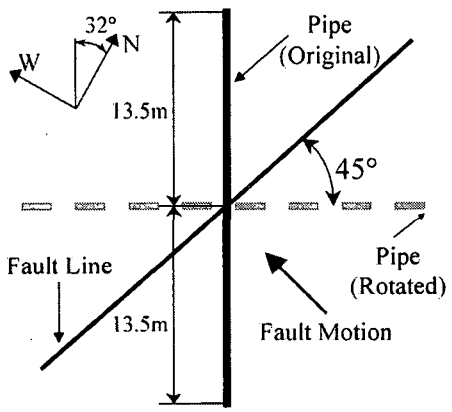

Fig. 2 Position of pipe; plan view (Fengyuan)

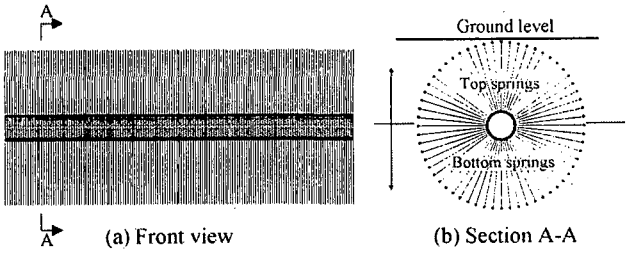

Fig. 3 Model of pipe considering interaction with soil

Table 1. Summary of analyses

No.	Ultimate strain [%]	D/t	Pipe position	Remark
A1	10	105	Original	Pipe only
A2	20	105	Original	Pipe only
A3	10	143	Original	Pipe only
A4	20	143	Original	Pipe only
A5	10	143	Rotated	Pipe only
A6	10	105	Rotated	Pipe only
A7	10	105	Rotated	Pipe+Soft soil
A8	10	105	Original	Pipe+Soft soil
A9	10	105	Rotated	Pipe+Hard soil

(2) Results and Discussion

The resistance capacity of the pipe to fault motion is represented by the time history of the reaction force in the axial direction during the faulting process as shown in Fig. 4. The typical failure modes are shown in Fig. 5.

Regarding the influence of pipe position, we can conclude that when the main direction of fault motion is close to the direction of pipe axis the damage potential is much bigger. This is confirmed by analyses A1 and A3 as compared to analyses A6 and A5 respectively, see Fig. 4 (a) and (b) respectively.

Regarding the influence of the ratio D/t we can conclude that for higher values the pipe is more vulnerable under a given fault motion, compare A5 to A6,Fig. 4 (c). This can be attributed to the easier initiation of local buckling leading to strain localisation and ultimately to failure. The difference in this case is crucial since in A5 we have complete failure, whereas in A6 failure is not observed. On the other hand, if we compare A1 and A3 shown in Fig. 4 (d), we can see that the failure occurs at approximately the same time (fault displacement), so from the limited number of analyses performed firm conclusions cannot be drawn as to the importance of D/t (bending stiffness). It is most likely that an optimum value of D/t exists ensuring sufficient resistance potential with reasonable amount of steel (cost).

The influence of pipe-soil interaction can be seen by comparing A6, A7 and A9, see Fig. 4 (e). The difference in response can be also seen in the deflected shapes. In the lack of interaction, the deformed shape of A6 is a smooth cubic curve whereas in the presence of interaction (A7 and A9) the deformed shapes are more irregular. In the case of A9 failure does occur near the end of analysis, while failure is not observed for A6 and A7. In general, interaction influences the deformation pattern and hence the failure mode. For the above three analyses it helps strain localisation and failure occurs so interaction has a negative effect in this case. This effect is smaller when the direction of fault motion is similar to the direction of the pipe axis as can be seen from analyses A1 and A8 shown in Fig. 4 (f). Here the interaction effect changes the location of failure but for both analyses failure occurs at approximately the same time (fault displacement).

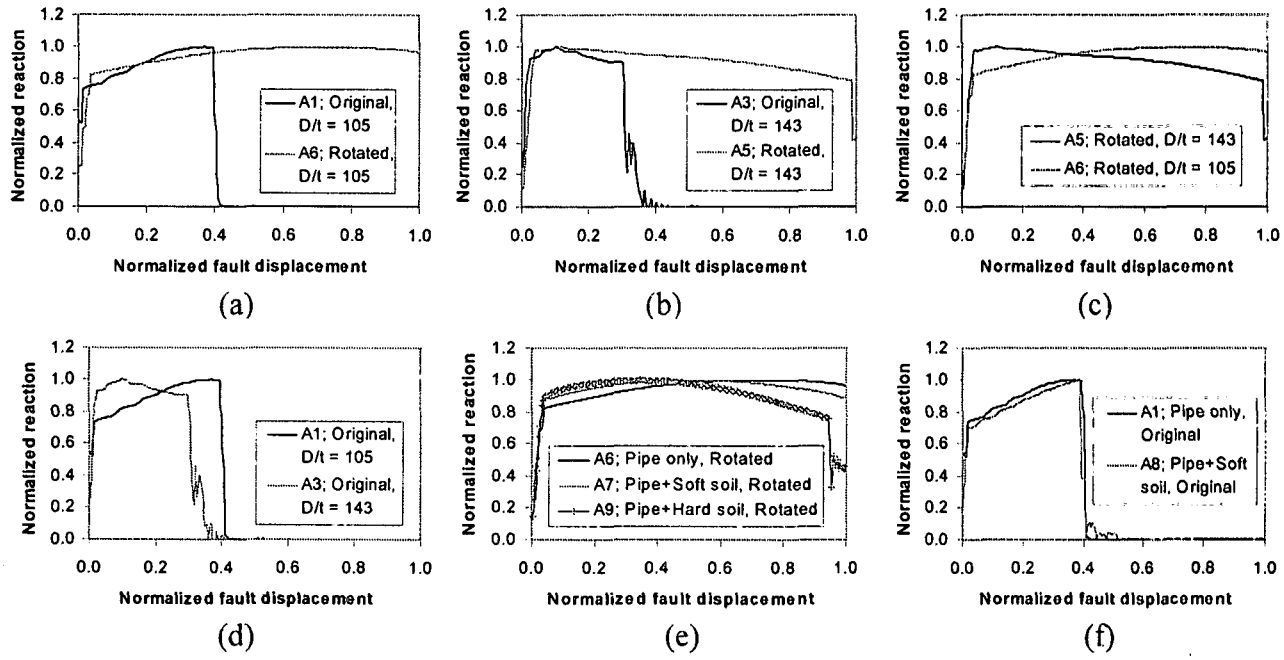

Fig. 4 Performance of analysed pipe (Fengyuan)

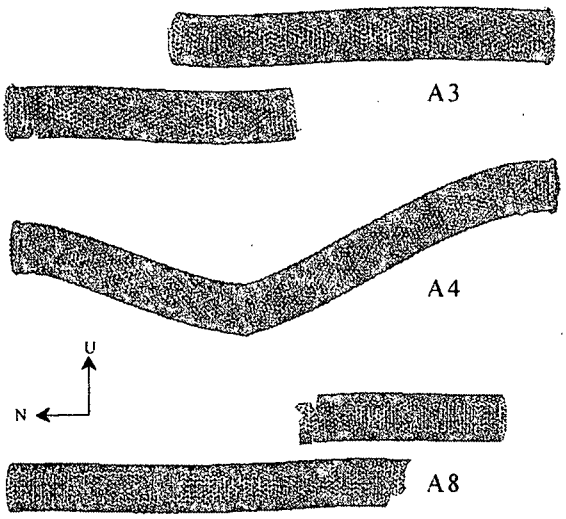

Fig. 5 Failure modes

Finally, a note on general deformation patterns. Pronounced local buckling was not observed here. This is because the model is long and deformations are smoothly distributed along the length. Another reason is perhaps that in the current version of the program plasticity in bending of walls is not considered.

5. CONCLUSIONS

A DEM modelling strategy that is computationally inexpensive compared to the typical DEM modelling approach was introduced.

The proposed procedure should be suitable for simulating the buckling behaviour of frames as well, both 2-D and 3-D. For the 3-D case the moments of inertia along two local principle axes have to be provided.

The analyses performed on pipes crossing active faults showed that local buckling should be avoided if we want to achieve the best performance from a pipe. Whereas failure cannot be avoided when excessive fault motion occurs, the ultimate differential displacement a pipe can sustain without damage can be increased significantly by using pipes of lower *D/t* when faults are crossed. In any case, an optimal value for the ratio *D/t* should be sought.

Fault motions with direction similar to the direction of pipe axis are were confirmed to be most damaging.

Pipe-soil interaction influences the behaviour in a negative way leading to strain localisation and hence to faster failure.

REFERENCES

1) Takada S. et al : 921 Chi-chi (Taiwan) earthquake, reconnaissance and relief work, *RCUSS*, pp. 2-9, 2000.

2) Ivanov R. I.: Failure analysis of structures by the three dimensional discrete element method, *Ph.D. Thesis*, Kobe University, 2001.

3) Takada S., Hassani N. and Ivanov R.: A hysteric model for reinforcement and its implementation in the 3-D discrete element method, *The Memoirs of Construction Engineering Research Institute* , Vol. 42-B, pp. 67-77, 2000.

4) Japanese Industrial Standards Committee: JIS G3443

5) Japan Gas Association: Guidance for seismic design of gas pipelines, pp. 376-377, 1982.

6) Katagiri S., Takada S. and Shinmi T.: Study on behaviour of buried corrugated pipelines subjected to large ground subsidence, Seismic ground motions; Response, repair and instrumentation of pipes and bridges, PVP-Vol. 227, pp. 73-78, 1992.